Maritime Technology and Research
https://so04.tci-thaijo.org/index.php/MTR

Research Article

Predictive models of non-optically active coastal water quality parameters by remote sensing imagery

Khaldoun Abualhin[1,*] and Soha Abushaban[2]

[1]*Department of Earth Science, Al Azhar University-Gaza, Gaza, Gaza Strip, Palestine*
[2]*Institute of Water and Environment, Al Azhar University-Gaza, Gaza, Gaza Strip, Palestine*

[*]*Corresponding author's e-mail address: khaldoun.alhin@gmail.com*

Article information
Received: September 2, 2024
Revision: December 24, 2024
Accepted: December 31, 2024

Keywords
Non-optically active;
Coastal water quality;
Empirical predictive models;
Multiple regression analysis;
Sentinel-2 MSI;
Dissolved oxygen

Abstract

The coastal waters of the Gaza Strip are significantly impacted by wastewater discharge and pollution from commercial and domestic activities. Timely monitoring and accurate assessment of water quality are crucial for detecting contamination. This study established correlations between spectral reflectance and non-optically active pollutants, specifically Dissolved Oxygen (DO), Total Phosphorus (TP), and Molybdenum (Mo). These parameters were selected for their relevance to wastewater pollution and compatibility with the employed measurement techniques. Non-optically active constituents, which do not exhibit distinct spectral signatures, may still be detectable under specific conditions. The study focused on testing the feasibility of retrieving concentrations of non-optically active components in seawater using Sentinel-2 MSI imagery. Sentinel-2 MSI was chosen for its high revisit frequency and broad wavelength range, making it suitable for assessing water quality. Empirical multiple regression models revealed varying performance among the pollutants. The TP model showed poor correlation and high uncertainty. In contrast, the predictive models for DO and Mo yielded more promising results. The DO model exhibited strong performance, achieving a significant coefficient of determination (R^2) value of 0.73, with a low prediction error: a Root Mean Square Error (RMSE) of 0.21 % and a Mean Absolute Percentage Error (MAPE) of 6.6 %. The Mo model demonstrated moderate accuracy, with an R^2 value of 0.51, an RMSE of 0.35 %, and a higher MAPE of 171 %. The results indicated that DO and Mo concentrations correlated with specific Sentinel-2 bands. This study confirms that remote sensing can effectively retrieve concentrations of non-optically active pollutants, supporting rapid seawater quality assessments, particularly in regions where field surveys are challenging.

1. Introduction

Declining water quality has serious implications, leading to reduced ecosystem productivity, and biodiversity loss, and adverse effects on aquaculture, agriculture, and other water-dependent sectors. Traditional water quality monitoring relies on in-situ measurements, sample collection, and laboratory analyses, which are often costly and labor-intensive. With the advent of remote sensing technology in the 1960s and 1970s, it became feasible to monitor pollutants and water components through their optical properties, such as reflection and absorption across various wavelengths. Since then, numerous algorithms have been developed for analyzing land and water quality, allowing remote sensing to become an effective tool for studying optically active water parameters. These

apparent optical properties (AOPs), like chlorophyll, suspended sediments, and dissolved organic matter, can be both qualitatively and quantitatively assessed to provide insight into water quality (Brezonik et al., 2015; Kim et al., 2016; Zeng et al., 2020). Despite advancements, monitoring non-optically active elements and pollutants through multispectral sensors remains challenging due to the unique characteristics of these elements. For instance, nutrients like Total Phosphorous (TP) and Total Nitrogen (TN), as well as indicators such as Chemical Oxygen Demand (COD), Biological Oxygen Demand (BOD), and Dissolved Oxygen (DO), generally lack direct optical signatures, making indirect remote assessment necessary (Guo et al., 2021; Pizani et al., 2020).

The coastal region of the Gaza Strip presents significant environmental challenges due to widespread pollution stemming from human activity, notably the discharge of untreated wastewater. Roughly 80 - 100 million cubic meters of wastewater are released into the Mediterranean annually, largely untreated due to limited treatment facilities and frequent power shortages (OCHA, 2018). This untreated wastewater degrades water quality, forming visible effluent plumes and contributing to widespread coastal pollution, making ongoing coastal monitoring crucial for quality assurance and hazard detection (Nahhal et al., 2021; PWA, 2012; USEPA, 2012). The absence of a tertiary treatment stage, and frequent interruptions in the treatment cycle caused by daily electricity shortages of more than 10 hours, hinder the effective treatment of wastewater. This results in unpleasant odors and the presence of turbid, dark wastewater effluent plumes in the surf zone, signaling significant coastal pollution. Monitoring such pollution, especially for elements with inactive apparent optical properties, remains challenging. For resource-constrained regions like Gaza, where traditional water quality assessment is often too costly and labor-intensive, there is an urgent need for alternative monitoring methods. Sentinel-2 satellite imagery presents a valuable solution by providing data that can be correlated with pollutants to enable broad-scale water quality monitoring. However, for non-optically active pollutants that interact minimally with light, accurate estimation through spectral characteristics remains difficult. Although only a limited number of studies have investigated the potential for monitoring non-optically active contaminants, such as TN, DO, TP, and COD, using satellite imagery, these studies can still serve as a valuable foundation for future research, as shown in **Table 1** (Fu et al., 2022; Gholizadeh & Melesse, 2017; Hassan et al., 2021; Mathew et al., 2017; Mushtaq & Nee Lala, 2017; Pizani et al., 2020; Zeng et al., 2020).

For example, Abayazid and El-Adawy (2020) demonstrated the feasibility of estimating DO in inland water using satellite imagery combined with multiple regression analysis of turbidity, total suspended solids (TSS), chlorophyll-a, and temperature. Gholizadeh and Melesse (2017) utilized best-fit multiple linear regression models, combined with ground data and Landsat TM and OLI imagery, to estimate TP and TN. Additionally, Zeng et al. (2020) demonstrated the spatial analysis of TP, COD, and other parameters using GaoFen-1 imagery, finding strong correlations for TP and COD within reservoirs. Ferdous and Rahman (2020) developed an empirical algorithm to monitor coastal water salinity using a combination of 13 different bands from Landsat TM and OLI data. The model accurately detected coastal water salinity for Landsat 5 and Landsat OLI, achieving R^2 values of approximately 0.82 and 0.76, respectively (Ferdous & Rahman, 2020).

Mushtaq and Nee Lala (2017) utilized the Normalized Difference Vegetation Index (NDVI) and Principal Component Analysis (PCA), in combination with in-situ measurements and spectral data from Landsat 8 OLI, to create a retrieval algorithm for non-optically active water quality parameters. Their analysis demonstrated a strong correlation between phosphate levels and NDVI, while pH and DO showed significant correlations with the first and fourth PCA components. González-Márquez et al. (2018) conducted multiple regression analysis using Landsat 8 spectral reflectance to estimate various water quality indicators, including non-optically active parameters

such as DO, electrical conductivity (EC), and pH. The analysis demonstrated reliable predictive capability, achieving R^2 values between 0.62 and 0.93, indicating the potential of remote sensing data for accurate estimation of these water quality metrics.

However, Sentinel-2 imagery was chosen for this study due to its key advantages in environmental monitoring. Its high to moderate spatial resolution and broad spectral range (13 bands, including red-edge bands) facilitate detailed analysis of coastal water quality, including non-optically active constituents. The satellite's frequent revisit time (every 5 days) ensures timely data acquisition, which is crucial for tracking dynamic environmental changes. Additionally, Sentinel-2 data is freely accessible, offering a cost-effective solution for large-scale monitoring. These features make it particularly suitable for developing empirical algorithms for seawater quality assessment. For Sentinel-2 imagery, Pizani et al. (2020) showed that four optically active parameters (chlorophyll-a, Secchi disk depth, turbidity, and temperature) could be used to indirectly assess non-optically active factors, achieving determination coefficients of 0.8 for DO. Karaoui et al. (2019) investigated the relationship between Sentinel-2 spectral characteristics and multiple water quality parameters. Their model successfully estimated DO and nitrate levels using Sentinel-2 imagery, achieving an R^2 value of approximately 0.52. The study by Fu et al. (2022) focused on evaluating optically active (OAPs) and non-optically active (NOAPs) water quality parameters in Poyang Lake using machine learning algorithms. Parameters such as TP, TN, ammonia nitrogen (NH4-N), and BOD5 were estimated. The study found that NOAPs had higher estimation accuracy than OAPs, with LOOCV-XG Boost and LOOCV-Gradient Boost outperforming SEL. Hassan et al. (2020) developed a hybrid model combining Binary Whale Optimization Algorithm and Artificial Neural Network to estimate optical and non-optical water quality parameters using Sentinel-2A data. The model addressed challenges of feature selection and low accuracy for non-optical parameters like TP. It achieved strong regression results, with R^2 values of 0.916 for optical and 0.890 for non-optical parameters.

Accordingly, this study aims to investigate key non-optically active parameters, TP, DO, and Mo, using Sentinel-2 imagery. The parameters are chosen for their strong associations with seawater pollution, particularly from sewage discharge. These parameters serve as critical indicators of coastal environmental health, reflecting nutrient loading and pollution impacts. Furthermore, the feasibility of measuring these parameters within the authors' institution's laboratory facilities enables accurate validation of remote sensing data against in-situ observations. By combining satellite imagery analysis with ground-based measurements, this study provides a comprehensive assessment of water quality and evaluates the efficacy of remote sensing as a tool for environmental monitoring in coastal zones.

1.1 Study area

The study focuses on the Gaza fishing port and its surrounding costal water, both of which are heavily impacted by wastewater pollution along the Gaza Strip's coastline. The area under investigation, illustrated in **Figure 1**, covers the northern coastal zone of Gaza City, extending approximately 6 km along the shoreline and about 1.5 km into the sea. The Gaza fishing port, located at decimal degree coordinates 31.5° N and 31.43° E, is a critical site for both economic and tourist activities, making it an important area for environmental monitoring.

The region is home to several wastewater discharge points, with two major outfalls serving a population of approximately 650,000 residents. Since 2016, these outfalls have been discharging roughly 60,000 m^3 of untreated wastewater per day into the coastal waters. This has led to the formation of a pollution plume that extends along Gaza City's shoreline, resulting in severe environmental consequences. Among the most notable impacts are high levels of eutrophication,

which contribute to declining water quality, beach erosion, and the degradation of marine ecosystems. Furthermore, the increasing pollution load has created health risks for both the local population and marine life, affecting biodiversity and local industries.

Water quality in the study area fluctuates significantly over both time and space. Reports indicate that the COD levels in the coastal waters range from 600 to 1,300 mg/l, reflecting high levels of organic pollution. Similarly, the BOD5 levels range from 470 to 800 mg/l, indicating the presence of substantial organic matter in the water. These values highlight the serious pollution challenges faced by the Gaza coastline and underscore the urgent need for effective environmental monitoring and management (Abualtayef et al., 2021; Nahhal et al., 2021; PWA, 2012; Shomar et al., 2005; Vestner et al., 2013).

Table 1 Recent studies highlighting the influential spectral bands for non-optically active parameters. (Information about spectral bands and central wavelength of both sensors presented in **Table 3**).

Sensor	Non-optical active parameter	Linear Regression R^2	Bands	Author
Sentinel-2	TP	0.65	B3, B4, B5, B6, B7, B8, B3, B4, B5, B6, B7, B8	Guo et al. (2021)
	TN	0.76		
	COD	0.81	B2, B3, B5, B6, B7, B8	
Landsat 8 OLI	EC	0.76	B2, B3, B4	Ferdous & Rahman (2020)
Sentinel-2	DO	0.741	B8, B9, B10, B11	Karaoui et al. (2019)
	Nitrate	0.67	B1, B2, B3, B9	
	Phosphate	0.54	B1, B3, B4, B5, B9, B10	
	TP	0.52	B02, B04, B07, B1	
Landsat 8 OLI	Phosphate	0.72	NDVI	Mushtaq & Nee Lala (2017)
	COD	0.49	B2	
	TDS	0.61	B6	
	DO	0.43	PCA	
	pH	0.61	PCA	
Landsat 8 OLI	EC	0.69	B2, B3, B4, B6	González-Márquez et al. (2018)
	pH	0.81	B3, B4, B5, B6	
	DO	0.93	B1, B3, B4, B5, B7	

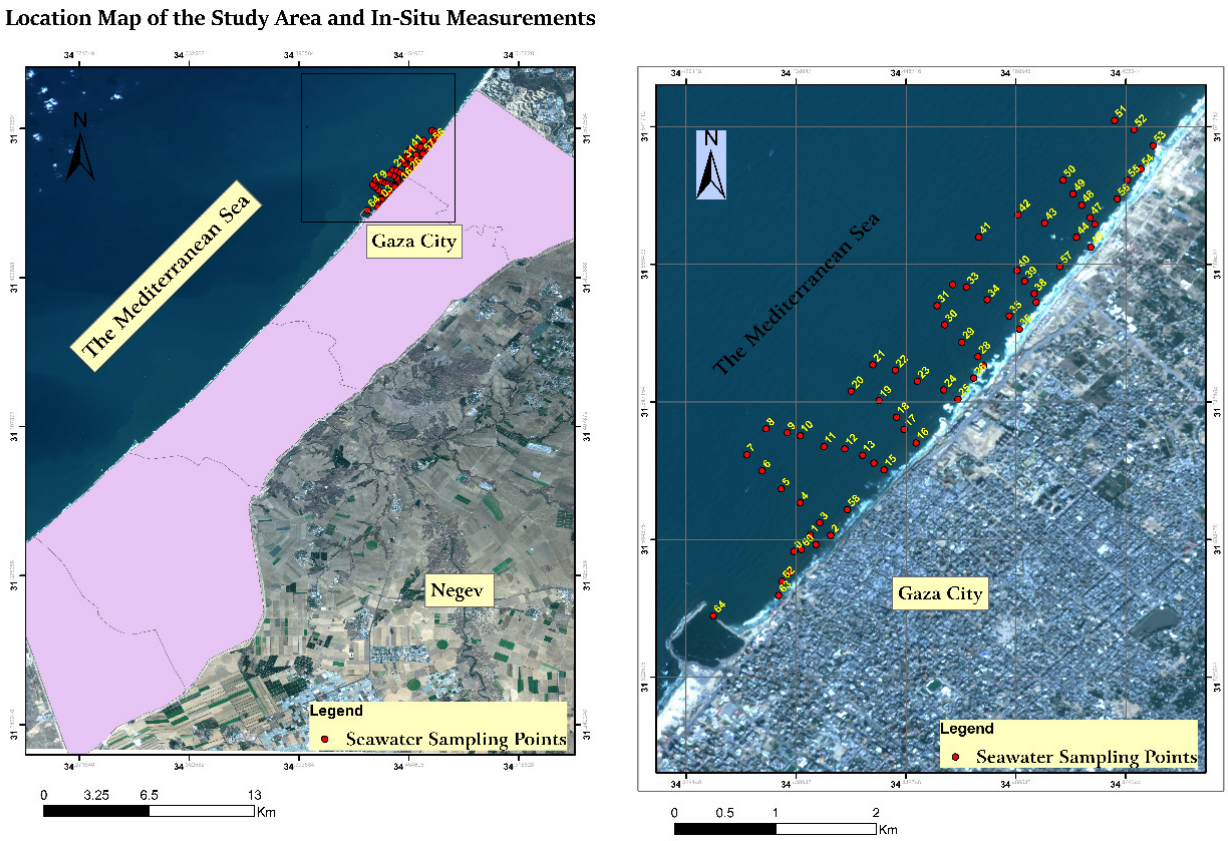

Figure 1 Location map of the study area, including in-situ measurement sites.

2. Research methodology

2.1 Field data collection

The research methodology integrates both fieldwork data collection and satellite-based remote sensing techniques to comprehensively assess seawater quality in the coastal waters of Gaza City. A set of surface seawater samples was collected along ten cross-shore transects during a boat survey on December 6, 2020. In-situ measurements were taken simultaneously with satellite overpasses of the study area. Seawater samples were gathered from 64 sites distributed throughout the coastal waters of Gaza City, as shown in **Figure 1**. During the in-situ measurements, the coordinates of each sampling point were recorded using a Garmin GPS device, which included four wastewater outlets within the study area. Field measurements included seawater clarity (as Secchi disc (SD)), water depth, and DO concentration. Seawater samples were collected in sterilized bottles and transported to the laboratory for analysis of TP and molybdenum. **Table 2** presents the list of measured seawater quality parameters. Sentinel-2B Level 1C imagery, captured on December 6, 2020, was downloaded from the from the Copernicus Open Access Hub. Image preprocessing was conducted using the Sentinel Application Platform (SNAP), where images were resampled to a 10-meter resolution and atmospherically corrected.

Table 2 Summary statistics of in-situ measurements for seawater DO, TP, and MO.

Parameter	Unit	Mean	S.D.	Maximum	Minimum
DO	mg/l	2.86	0.48	3.89	2.04
TP	mg/l	1.90	0.31	2.60	1.50
Mo	mg/l	0.56	0.48	9.00	0.10

2.1.1 *In-situ* DO

DO is a critical parameter for assessing seawater quality, as oxygen deficiency is indicative of severe pollution and can significantly impact aquatic life (Gholizadeh & Melesse, 2017). The influx of nutrients and organic matter, such as hydrocarbons from wastewater effluents and the fishing industry, contributes to eutrophication, which can further lead to oxygen depletion. During this process, oxygen is consumed, resulting in hypoxic or anoxic conditions in the water body (Salomon & Markus, 2018). Therefore, it is essential to regularly monitor temporal and spatial changes in DO patterns in coastal waters. In Gaza City, in-situ measurements of DO concentrations were conducted using a DO probe, yielding values ranging from 2.04 to 3.89 mg/l. The maximum allowable concentration for fisheries and aquatic life, according to European Union (EU) standards, is between 5 and 9 mg/l (Chapman et al., 1996).

2.1.2 *In-situ* TP

Phosphorus is an essential nutrient component found in nonpoint source runoff, agricultural runoff, and domestic wastewater effluents. While nutrient inputs to coastal waters are necessary for maintaining a healthy aquatic ecosystem, elevated nutrient concentrations can lead to increased algal growth, eutrophication, reduced water clarity, benthic degradation, and decreased DO levels. Phosphorus concentrations are typically measured as orthophosphates (PO_4-P), total inorganic phosphate, or TP, with natural water bodies generally exhibiting concentrations ranging from 0.005 to 0.020 mg/l (Chapman et al., 1996). The PO_4 molecule is three times as heavy as the phosphorus (P) atom; thus, results reported as PO_4 are three times the concentration of those reported as P. To convert PO_4 to P, the reported value must be divided by three (Eaton et al., 2012). In the laboratory, collected seawater samples were filtered to eliminate color and remove suspended matter. The TP concentrations in the coastal waters of Gaza City were measured using the spectroscopy method, with results ranging from 1.5 to 2.6 mg/l.

2.1.3 *In-situ* Mo

Mo is an essential trace element for various life forms, but exposure to elevated levels can be harmful. In most seawater, Mo is found at trace levels of less than 10 µg/l (Smedley & Kinniburgh, 2017). Mo is a stable metal used in the production of steel for vehicle bodies, steel alloys, welding rods, lubricant additives, corrosion inhibitors, pigments, and ceramics (Morrison et al., 2006). Mo can be released into the environment through the reductive dissolution of manganese and iron oxides or through the degradation of organic matter (Smedley & Kinniburgh, 2017). It is relatively unreactive in seawater and tends to concentrate in anoxic waters or near anoxic sediments. Measurements of Mo were obtained using UV-VIS spectrophotometry, with concentrations ranging from 0.1 to 9 mg/l. The highest concentration, approximately 9 mg/l, was found at Al-Shatti Camp, an area where wastewater outlets and the remains of galvanized steel gabion cages are present. In the northern coastal waters of Gaza City, Mo concentrations were generally low in various areas of the study site. The presence of Mo may be attributed to the groins constructed from building debris, which often contains paints and pigments.

2.2 Sentinel-2 imagery acquisition and pre-processing

Sentinel-2 is an Earth observation satellite system that includes the Sentinel-2A and Sentinel-2B satellites, which were launched on June 23, 2015, and March 7, 2017, respectively. Key reasons for selecting Sentinel-2 include its favorable revisit time and coverage, free accessibility for data downloads, and broad electromagnetic spectrum coverage from visible to shortwave infrared (SWIR). These features make it particularly suitable for developing empirical algorithms for seawater quality assessment. A cloud-free Sentinel-2B Level-1C satellite image was obtained from the Copernicus Open Access Hub and processed using the Sentinel Application Platform (SNAP). Detailed specifications for the Sentinel-2 bands are provided in **Table 3**, with wavelengths ranging from 443

nm to 2,190 nm. The image was acquired on November 6, 2020, at 09:24:25 AM UTC. The Sentinel-2B Level-1C image underwent radiometric and geometric corrections using a digital elevation model (DEM) to correct for ground geometric distortions. Pixel radiometric measurements are provided in Top-Of-Atmosphere (TOA) reflectance (ESA, 2021). The Multispectral Instrument (MSI) is the sole optical instrument payload carried by the Sentinel-2 spacecraft, featuring band specifications similar to those of the Landsat-8 Operational Land Imager (OLI) (Segl et al., 2015). Atmospheric correction is a critical step in obtaining surface reflectance, as it removes atmospheric interference from the overall signal captured by the satellite sensor. Consequently, TOA reflectance was converted to surface reflectance by applying the atmospheric correction algorithm (FLAASH), which is incorporated into ENVI software. The atmospherically corrected image was then resized, and a land mask was applied. Satellite imagery from Sentinel-2B captures data at different spatial resolutions: 10 m for the visible and near-infrared bands, 20 m for the red-edge and shortwave infrared bands, and 60 m for the atmospheric bands. To facilitate spectral data extraction for statistical modeling, all Sentinel-2B bands were rescaled to a uniform 10 m resolution. This rescaling ensures consistency across the dataset, which is essential for effective comparative analysis and integration with in-situ measurements. By adjusting the higher resolution bands to 10 m, coherence was maintained among all bands, which is critical for accurate modeling and interpretation of the data.

Table 3 Spectral bands of Sentinel-2 MSI.

Band number	Central wavelength (nm)	Bandwidth (nm)	Spatial resolution (m)	Landsat 8 OLI	Central wavelength (nm)
B 1 - Coastal aerosol	443	20	60	B1	433
B 2 - Blue	490	65	10	B2	450
B 3 - Green	560	35	10	B3	530
B 4 - Red	665	30	10	B4	670
B 5 - Red-edge	705	15	20	-	-
B 6 - Red-edge	740	15	20	-	-
B 7 - Red-edge	783	20	20	-	-
B 8 - NIR	842	115	10	-	-
B 8a - NIR	865	20	20	B5	860
B 9 - Water vapor	945	20	60	-	-
B 10 - Cinus	1,375	30	60	-	-
B 11 - SWIR	1,610	90	20	B6	1,600
B 12 - SWIR	2,190	180	20	B7	2,200

2.3 Development of empirical models

Empirical model development is a widely used method for establishing direct correlations between input and output variables, specifically, the spectral reflectance of multispectral bands and the in-situ measurements. Reflectance values for image pixels were extracted from the corresponding in-situ measurement locations. Given the short residence time of coastal water, a tolerance of 2 to 4 hours was selected to align the satellite overpass time with the in-situ measurements of water constituents. This alignment enhanced the reliability of the findings by minimizing variations in seawater quality due to environmental changes over time. To exclude outliers, Tukey's rule was applied, which identifies outlier values as those exceeding a distance of 1.5 times the interquartile range from either the first or third quartiles (Wilcox, 2010). To account for spatial variations between GPS sampling points and satellite pixel sizes, as well as the rapid dynamics of coastal waters, a smoothing filter (3×3 kernel) was applied to the entire image before retrieving pixel values

(Lubczonek & Zaniewicz, 2023). A comprehensive set of 192 tests was conducted to evaluate three parameters. Out of these, 101 tests were used in constructing prediction models via multivariate statistical analysis. After removing zero values and outliers, 34 tests remained to assess the accuracy of the prediction models. Various algorithmic approaches have been developed to obtain water quality parameters from remote sensing data. One such approach is the empirical method, or experimental algorithmics, which utilizes statistical techniques to establish relationships (Dierssen, 2010; Matthews, 2011; Yu et al., 2019).

Local empirical algorithms developed from in-situ measurements are often proposed to enhance prediction accuracy from remotely sensed imagery. To establish an empirical prediction model, the independent variables (spectral information from pixels) are plotted against the dependent variables (concentrations of seawater quality parameters) in a scatter plot, followed by regression analysis to derive coefficients. Linear regression analyses were conducted for each individual spectral band in relation to the observed water quality parameters, producing R^2 values for each band. The band with the highest R^2 value was identified as the most effective predictor of the observed parameters and was subsequently selected for multiple regression analysis. This approach ensured that the model focused on the band that best explained the variance in water quality. Following this selection, multiple linear regression analysis was performed, incorporating the selected band and other relevant independent variables to develop the final model equation.

Although linking remote sensing data to non-optical water quality elements remains a contentious issue, numerous studies have demonstrated the potential to investigate certain non-optical elements through the indirect effects of compounds associated with their presence, which may exhibit detectable optical properties. **Figure 2** illustrates the methodological flowchart, depicting the sequence of activities involved in the empirical algorithm development process.

2.4 Correlation and multiple regression analysis

Correlation and regression analyses were employed to examine the relationships and collinearity between dependent and independent variables. Multicollinearity refers to a situation in regression analysis where two or more independent variables are highly correlated, leading to redundancy in the data. This redundancy can undermine the model's predictive power and interpretability, as it becomes challenging to isolate the individual effects of each predictor. In this study, a correlation matrix was employed to assess multicollinearity among the independent variables, facilitating the identification of pairs of predictors with high correlation. By addressing multicollinearity, the reliability of the regression model was improved. Linear regression and band-ratio transformation models were utilized to derive prediction models. The R^2 values for water quality values and spectral reflectance values were initially calculated. The R^2 values indicates the proportion of variation in the dependent variable predicted by the statistical model. A significance level of 95 % with p-value < 0.05 was established. To reduce redundancy among variables, those with high coefficients of determination were selected for multiple regression analysis. Multiple linear regression (MLR) was performed to model the linear relationship between the mean spectral reflectance of Sentinel-2 MSI bands (independent variables) and the in-situ measured values of water quality parameters (dependent variables). Both optical and non-optical seawater quality parameters were investigated as dependent variables. The independent variables for the regression model included spectral bands from Band 1 to Band 9 (**Table 3**), while bands associated with atmospheric effects and temperature (Bands 8a, 10, 11, and 12) were excluded.

Simple linear regression employs one independent variable, while multiple linear regression incorporates multiple independent variables. In similar studies, single bands, band-ratios, and combinations of multiple bands have been commonly utilized as independent variables in multiple linear regression analyses (Abualhin & Niemeyer, 2018; Gons, 1999; Matthews, 2011; Meer et al., 2014; Morel & Gentili, 2009).

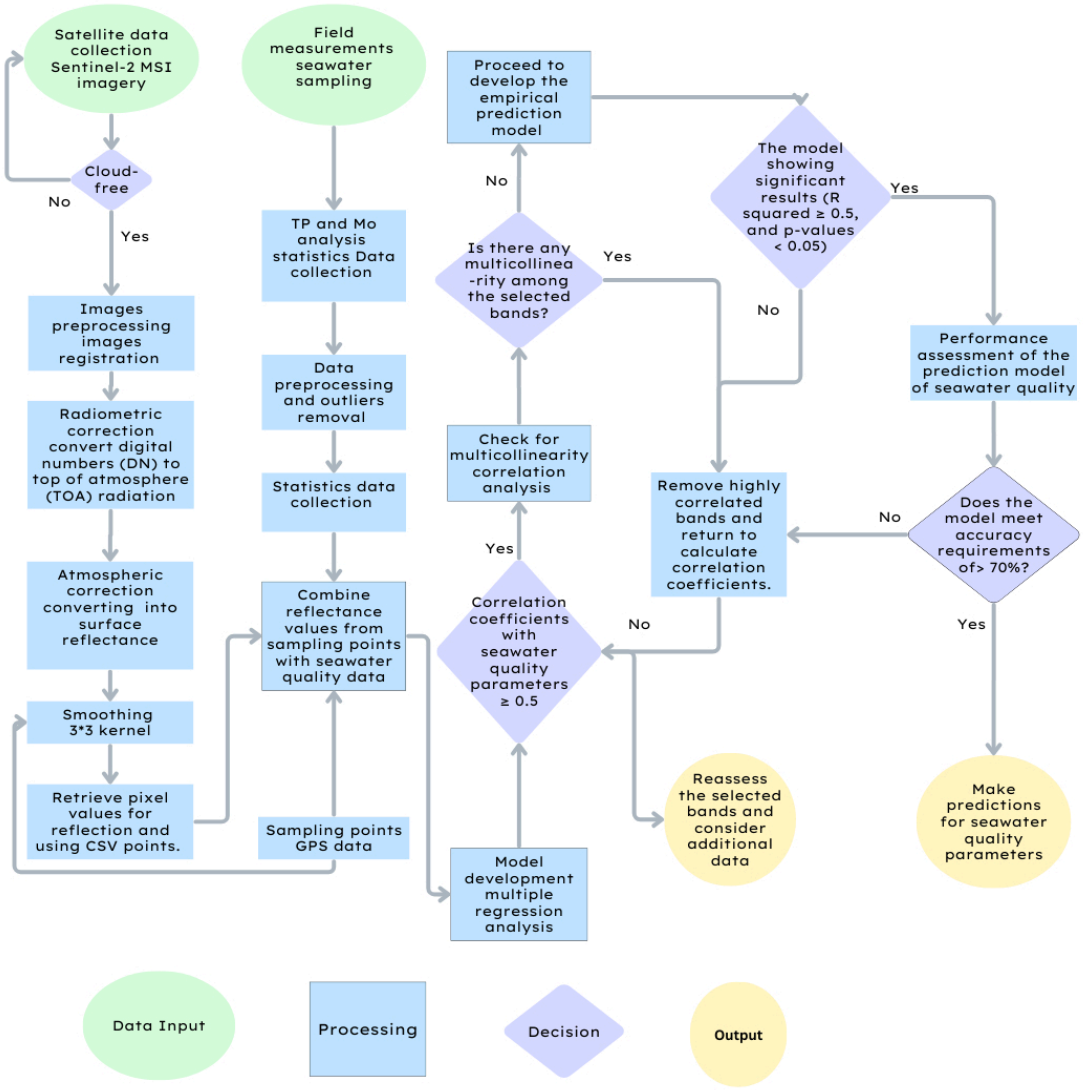

Figure 2 Flowchart depicting the sequence of steps involved in developing the empirical predictive algorithm for non-optically active elements.

3. Results and discussion

This study utilized linear and multiple regression models to examine the relationships between water quality parameters (as dependent variables) and spectral reflectance values (the independent variable) from Sentinel-2 MSI data. The focus was on the statistical associations between spectral bands and concentrations of TP, DO, and Mo. Key statistical indicators, including R^2, correlation coefficient (r), and the P-value, were analyzed to assess model effectiveness and significance.

3.1 Predictive model of TP

In examining the relationship between spectral reflectance and TP concentration, multiple regression analysis revealed significant correlations between specific spectral bands and TP levels. **Table 4** summarizes r and R^2 values for each band. The spectral bands B3, B7, and B8 displayed correlations with TP, with r values of 0.61, 0.54, and 0.51, respectively, and corresponding R^2 values of 0.37, 0.29, and 0.26, respectively. These results emphasized a weak predictive potential for TP concentration. **Figure 3** illustrates the linear regression analysis between band B3 and TP concentration, highlighting that the model lacks the robustness needed for reliable prediction of TP concentration based solely on spectral reflectance. Accordingly, a predictive model could not be derived for TP, and the process for TP was terminated at this stage.

Table 4 Regression coefficients between Sentinel-2 spectral bands and TP concentration.

Spectral bands	r	R^2
B1	0.36	0.13
B2	0.32	0.10
B3	0.61	0.37
B4	0.43	0.18
B5	0.43	0.18
B6	0.49	0.24
B7	0.54	0.29
B8	0.51	0.26
B9	0.45	0.20

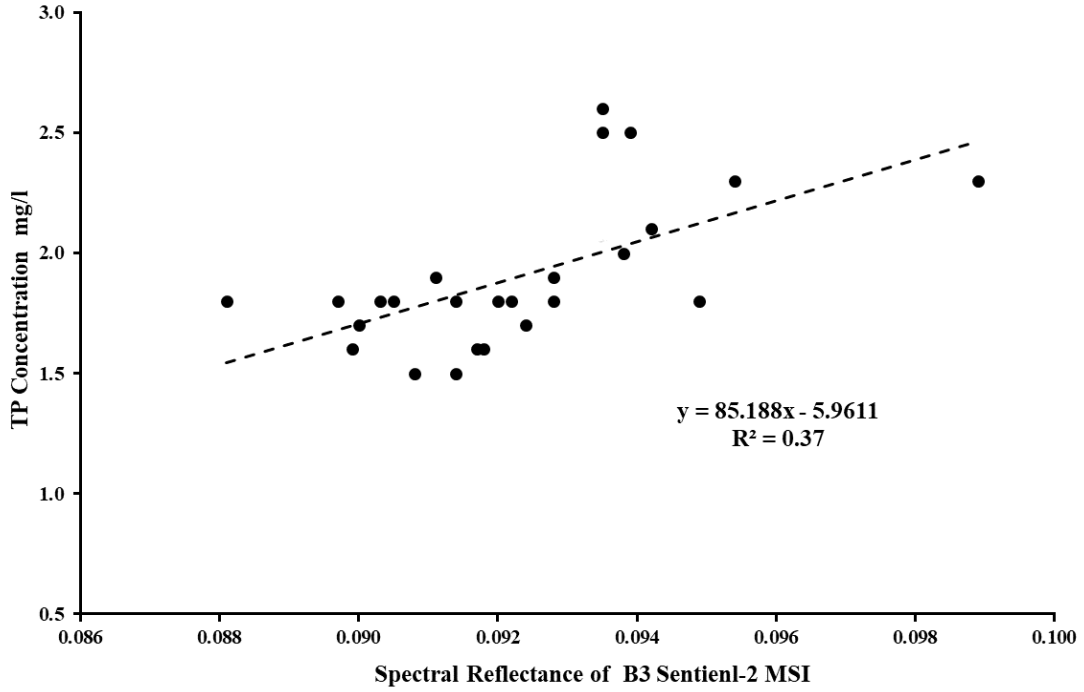

Figure 3 Linear regression analysis between Sentinel-2 B3 and TP concentration, demonstrating the weak correlation observed in the dataset.

3.1.1 Predictive model of DO

The reflectance values from Sentinel-2 bands were correlated with in-situ DO concentrations using linear regression analysis. In this study, two distinct approaches were used to develop predictive models for DO concentration using Sentinel-2 spectral data: (1) a multiple regression model incorporating three key spectral bands with strong correlation, and (2) a single-band regression model based on the band with the highest individual correlation.

3.1.2 Developing a DO predictive model using the multiple regression

The first approach used multiple regression analysis to develop a predictive model based on the spectral bands B1, B2, and B3, which showed the highest individual correlations with in-situ DO

concentrations. The simple linear regression analysis revealed strong positive correlations between the DO measurements and the Sentinel-2 spectral bands, as per **Table 5**. As shown in **Figure 4**, this model achieved a high R^2 value of 0.73 and a multiple correlation coefficient (r') = 0.85, and a P-value < 0.05, indicating a robust predictive relationship, as per **Table 6**. This model is represented by the following equation;

$$DO = -21.2535 + \big(23.96945 \times (B1)\big) + \big(161.0584 \times (B2)\big) + (14.51334 \times (B3)) \quad (1)$$

By combining data from these three bands, the multiple regression model offers an enhanced prediction capability for DO concentration. This approach may be particularly useful for more accurate DO monitoring across diverse water bodies.

Table 5 Regression coefficients among Sentinel-2 spectral bands and DO concentration.

Spectral bands	r	R^2
B1	0.75	0.56
B2	0.85	0.72
B3	0.66	0.44
B4	0.34	0.12
B5	0.34	0.12
B6	0.44	0.19
B7	0.50	0.25
B8	0.52	0.27
B9	0.49	0.24

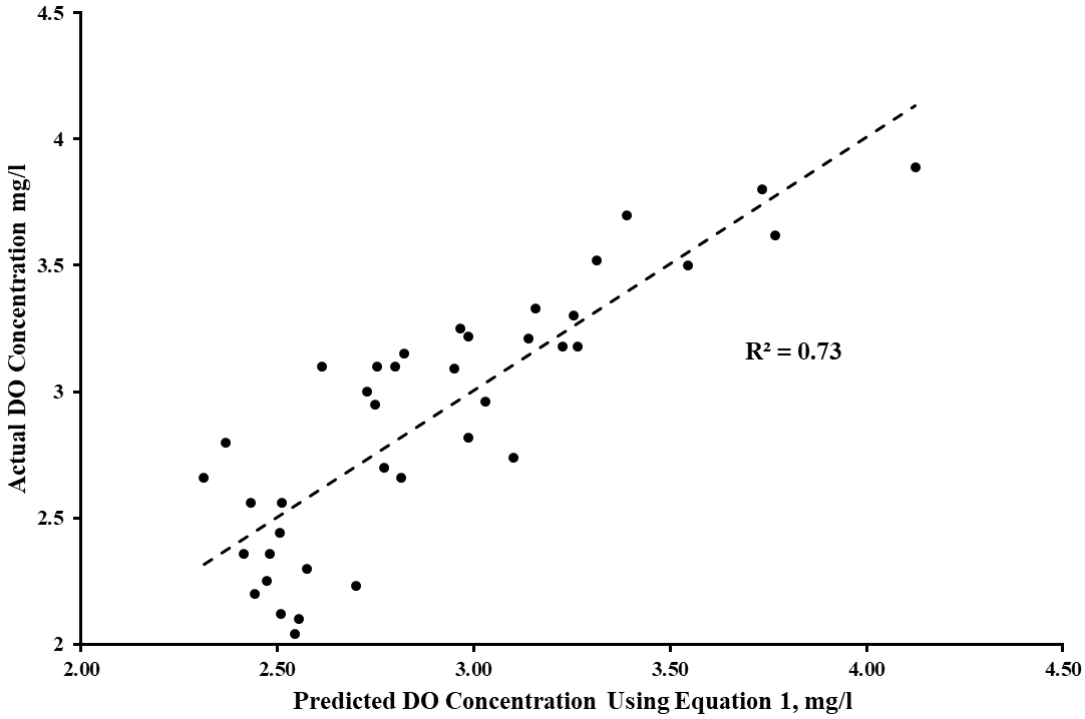

Figure 4 Scatter plot illustrating the DO predictive model based on Eq. (1). The X-axis represents predicted DO concentrations, while the Y-axis shows in-situ measured DO concentrations.

Table 6 Multiple regression coefficients for DO predictive model, Eq. (1).

Multiple r'	R^2	*P-Value*
0.85	0.73	5.64E-10

3.1.3 Developing a DO predictive model using the single-band regression

The second approach focused on developing a simpler predictive model using only the spectral band with the highest correlation to DO concentration, which was the blue band (B2). The single-band model, illustrated in **Figure 5**, showed a strong individual correlation with DO, with R^2=71 and a significant P-value < 0.05. The corresponding predictive equation for DO concentration using B2 is;

$$DO = \big(200.88 \times (B2)\big) - 21.065 \quad (2)$$

This single-band model offers a practical option for estimating DO levels using only B2 data, especially in scenarios where access to full spectral datasets is limited. This approach could facilitate efficient remote monitoring of DO concentrations using Sentinel-2 data, particularly in regions where in-situ measurements are challenging to obtain.

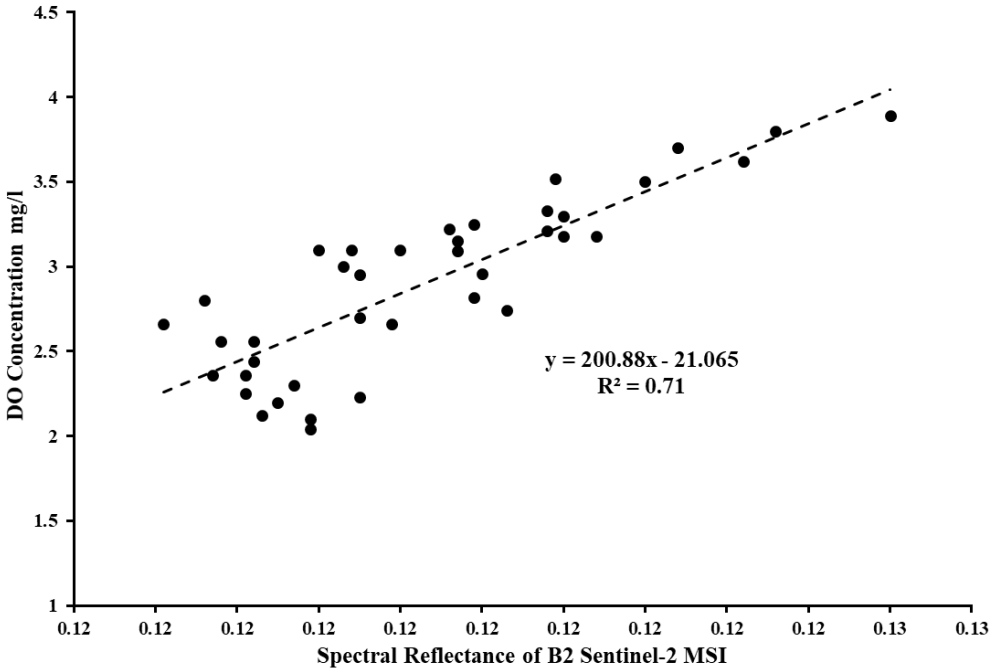

Figure 5 Linear regression between Sentinel-2 blue spectral band B2 and DO concentration.

Both models demonstrated effective predictive capabilities for DO concentration based on Sentinel-2 spectral data. The multiple regression model Eq. (1) provides improved accuracy by incorporating multiple spectral bands, while the single-band model Eq. (2) offers a streamlined alternative with strong predictive value based on the blue wavelength alone. These models highlight the potential of Sentinel-2 data for remote DO monitoring, supporting applications in environmental assessment and historical water quality analysis.

3.2 Predictive model of Mo

This study examined the relationship between Sentinel-2 spectral reflectance and Mo concentrations in coastal waters. Two predictive modeling approaches were evaluated: a multiple

regression model based on selected spectral bands, and a band-ratio transformation model to address variations in illumination and enhance prediction accuracy.

3.2.1 Developing a Mo predictive model using multiple regression

A multiple linear regression model was developed using the Sentinel-2 red-edge spectral bands (B6, B7, and B8) along with NIR B9 and the Mo in-situ measurements. These bands were chosen based on their individual r values of 0.69, 0.65, 0.63, and 0.7, respectively, as shown in **Table 7**. The multiple regression analysis of these bands produced a robust predictive model, with an r' value of 0.81, an R^2 value of 0.65, and a significant P-value of < 0.005, **Table 8**. The Mo predictive model is represented by Eq. (3);

$$Mo = -3.955 + (468.837 \times (B6)) + (-312.708 \times (B7)) + (-174.603 \times (B8)) + (152.531 \times (B9)) \quad (3)$$

Table 7 Regression coefficients between Sentinel-2 spectral bands and Mo concentration.

Spectral bands	r	R^2
B1	0.36	0.13
B2	0.17	0.03
B3	0.49	0.24
B4	0.55	0.30
B5	0.59	0.35
B6	0.69	0.48
B7	0.65	0.42
B8	0.63	0.40
B9	0.7	0.49

The multiple regression model demonstrated a strong association between Mo concentrations and these spectral bands, as shown in **Figure 6**. This model could serve as an empirical tool for estimating Mo levels in coastal waters using Sentinel-2 red-edge and near-infrared reflectance data.

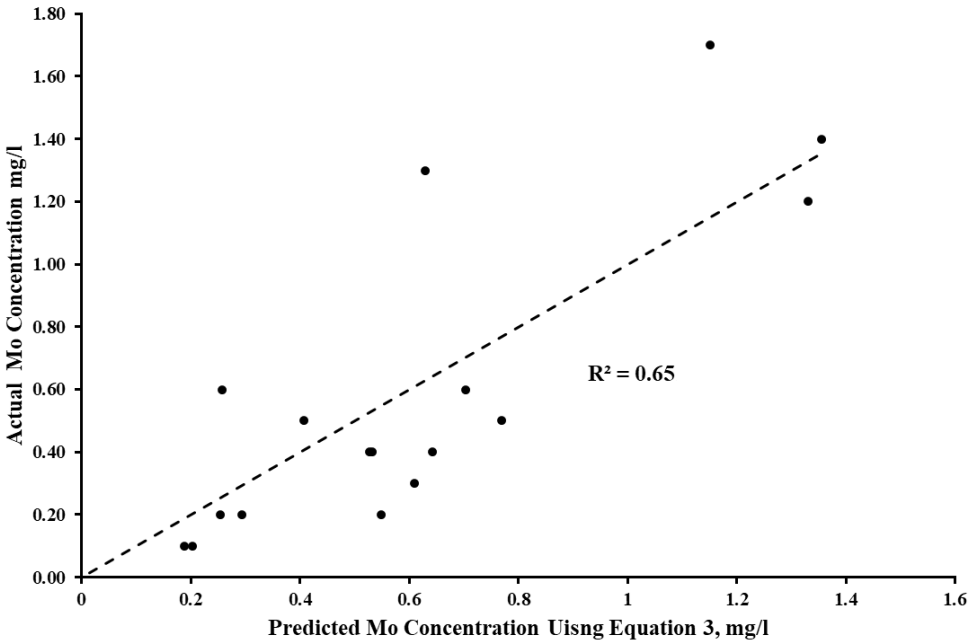

Figure 6 Scatter plot illustrating the Mo predictive model based on Eq. (3). The X-axis represents predicted Mo concentrations, while the Y-axis shows in-situ measured Mo concentrations.

Table 8 Multiple reflectance values for regression coefficients between Mo concentration and spectral bands: B6, B7, B8, and B9.

Multiple r'	R^2	*P-Value*
0.81	0.65	0.0055

3.2.2 Developing a Mo predictive model using the band-ratio

To further improve prediction accuracy, a second model was developed using band-ratio transformations. Band ratio processing helps minimize the effects of varying illumination and enhances spectral differences, particularly in optically complex coastal waters (Doxaran et al., 2002; Gupta, 2017; McKee et al., 2007; Sun et al., 2014). After testing several band combinations, the ratios B2/B3, B2/B8, and B3/B8 were found to have the strongest inverse associations with Mo concentrations, with r values of -0.65, -0.71, and -0.67, respectively, as per **Table 9**.

The predictive model based on these band-ratios achieved a moderate association, with an r' value of 0.72, an R^2 value of 0.52, and a significant P-value < 0.05, **Table 10**. The band-ratio based prediction model for Mo concentration is described by Eq. (4);

$$\mathrm{Mo} = -12.36 + \left(12.6 \times \left(\frac{\mathrm{B2}}{\mathrm{B3}}\right)\right) + \left(-5.1 \times \left(\frac{\mathrm{B2}}{\mathrm{B8}}\right)\right) + \left(5.67 \times \left(\frac{\mathrm{B3}}{\mathrm{B8}}\right)\right) \quad (4)$$

Table 9 Regression coefficients between Sentinel-2 spectral band-ratios and Mo concentration.

Spectral band-ratio	*r*	*B2/B3*	*B2/B4*	*B2/B8*	*B3/B4*	*B3/B8*
B2/B3	-0.65	1.00				
B2/B4	-0.56	0.87	1.00			
B2/B8	-0.71	0.82	0.86	1.00		
B3/B4	-0.49	0.75	0.98	0.81	1.00	
B3/B8	-0.67	0.71	0.79	0.98	0.77	1.00
B4/B8	-0.49	0.25	0.11	0.60	0.05	0.67

Table 10 Multiple regression coefficients for the band-ratio prediction model of Mo concentration.

Multiple r'	R^2	*P-Value*
0.72	0.52	0.013

As illustrated in **Figure 7**, this model provides a feasible method for estimating Mo concentrations using band-ratios, which may be particularly useful in environments with high optical complexity.

Both modeling approaches demonstrated a moderate predictive capability for Mo concentration. The multiple regression model Eq. (3), which leverages red-edge and near-infrared bands, offers better prediction accuracy, while the band-ratio model Eq. (4) provides a practical alternative that is less sensitive to variations in light conditions. These models can be applied to remotely monitor Mo concentrations in coastal environments and can potentially inform water quality assessments in regions where direct sampling is challenging.

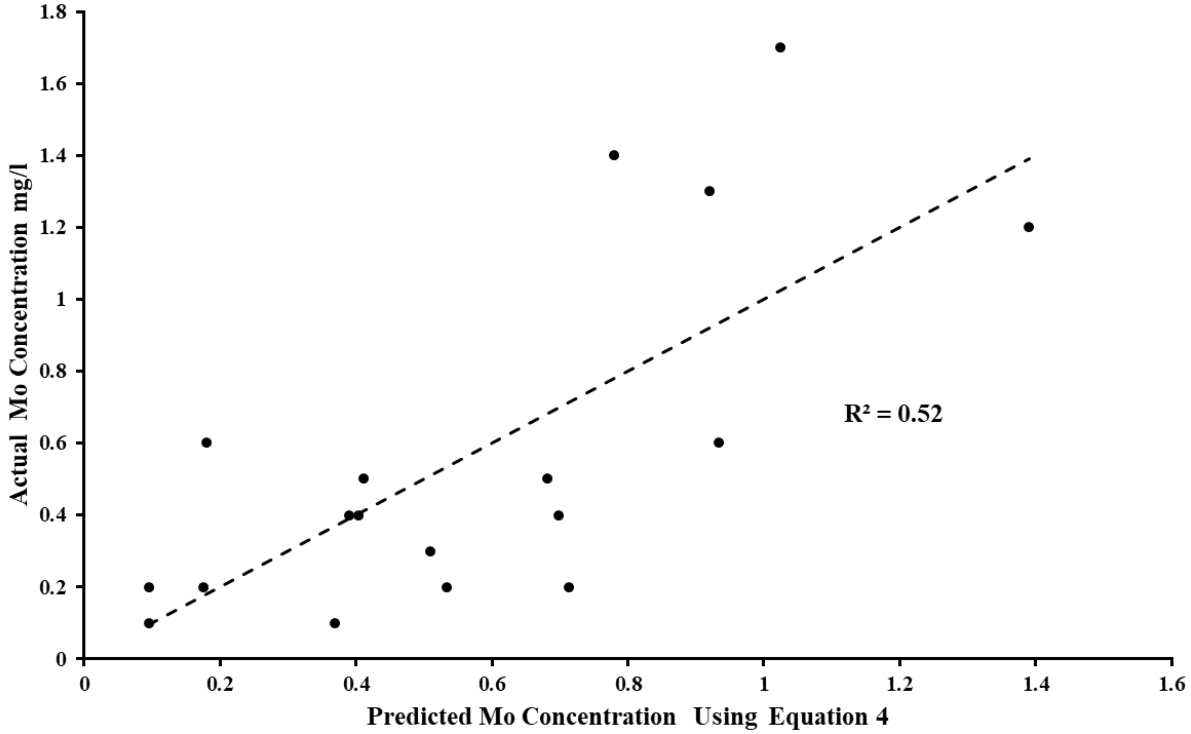

Figure 7 Scatter plot illustrating the Mo predictive model based on Eq. (4). The X-axis represents predicted Mo concentrations, while the Y-axis shows in-situ measured Mo concentrations.

3.3 Implementation and evaluation of the prediction models

This section presents the application and evaluation of the empirical prediction models developed for DO and Mo concentrations in the coastal waters of the Gaza Strip. The models were applied to Sentinel-2 images to predict these water quality parameters, while TP was excluded due to its weak correlation with the spectral data, rendering it unsuitable for reliable model development. A cross-validation accuracy assessment method was employed in this study.

3.3.1 The DO predictive model evaluation

The predictive models for the DO Eqs. (1) and (2) were applied to the study area, and their accuracy was assessed through three key metrics: the R^2, RMSE, and MAPE. The results are summarized in **Table 11**. RMSE quantifies the average magnitude of prediction errors, where lower values signify better model performance, while MAPE expresses the error as a percentage of the observed values.

3.3.1.1 Model performance: Eq. (1) exhibited a considerable accuracy, with an R^2 value of 0.73, meaning it explained 73 % of the observed variance in DO concentrations, as per **Figure 8**. This was significantly higher than Eq. (2), which had an R^2 of 0.53. The RMSE for Eq. (1) was 0.21 %, indicating low prediction error, while the MAPE was 6.6 %, further highlighting its accuracy compared to Eq. (2) (MAPE = 9.2 %), as per **Figure 9**. These accuracy metrics collectively show that Equation 1 was the better model for predicting DO concentration.

3.3.1.2 DO distribution: Using Eq. (1), a predictive map was generated for DO concentrations across the Gaza Strip. The map (**Figure 12**) revealed that the coastal waters generally exhibit low oxygen levels, with hypoxic conditions (DO < 2 mg/L) prevalent in areas, particularly near wastewater disposal sites. These hypoxic zones are concerning as they indicate contamination from untreated wastewater, which can severely impact marine life, especially in areas where oxygen levels fall below 4 mg/L.

Table 11 Accuracy assessment of the DO predictive models using Eqs. (1) and (2).

DO predictive model	R^2	*RMSE %*	*MAPE %*
Eq. (1)	0.73	0.21	6.60
Eq. (2)	0.53	0.30	9.20

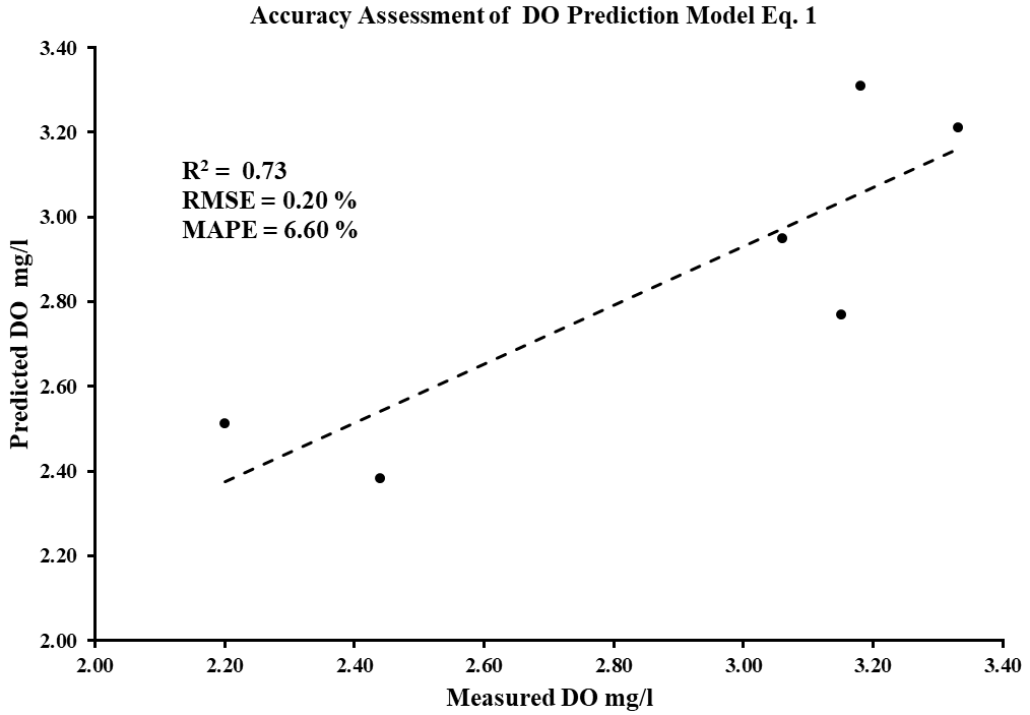

Figure 8 Accuracy assessment of the DO predictive model for Eq. (1).

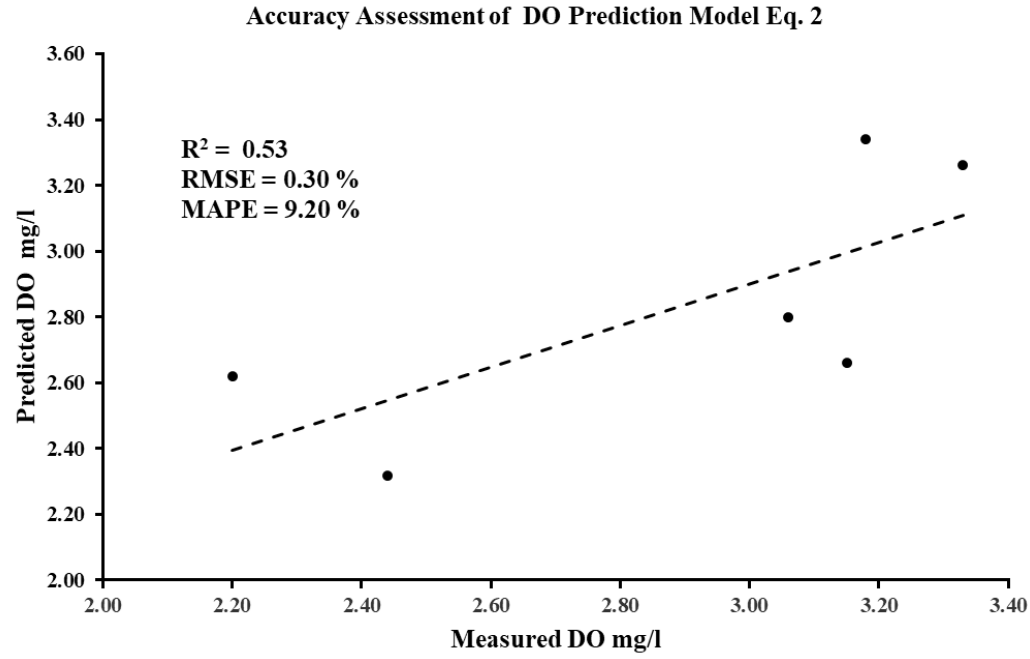

Figure 9 Accuracy assessment of the DO predictive model for Eq. (2).

3.3.2 The Mo predictive model evaluation

The accuracy of the predictive models for Mo Eqs. (3) and (4) was also evaluated using the same metrics (R^2, RMSE, and MAPE). The results, shown in **Table 12**, suggest that these models were less accurate than the DO models.

3.3.2.1 Model performance: For Eq. (3), the R^2 was 0.51, indicating that the model explained only 51 % of the variance in Mo concentration, as per **Figure 10**. The RMSE was 0.35 %, and the MAPE was alarmingly high at 171 %, suggesting considerable error, likely due to the low concentrations of Mo in the region. Eq. (4) performed slightly worse, with an R^2 of 0.33, RMSE of 0.31 %, and a MAPE of 37 %, as per **Figure 11**.

3.3.2.2 Mo distribution: Despite the relatively high error margins, Eq. (4) was used to generate a predictive map for Mo concentrations, as per **Figure 13**. The model showed that Mo concentrations in the Gaza Strip's coastal waters averaged 0.26 mg/L, with the highest concentrations (2 - 4 mg/L) located near shorelines and coastal structures. These elevated levels are likely associated with the degradation of steel and construction materials, as well as potential pollution from wastewater discharges.

Table 12 Accuracy assessment of the Mo predictive models using Eqs. (3) and (4).

Mo predictive model	R^2	*RMSE %*	*MAPE %*
Eq. (3)	0.51	-0.35	171
Eq. (4)	0.33	-0.31	37

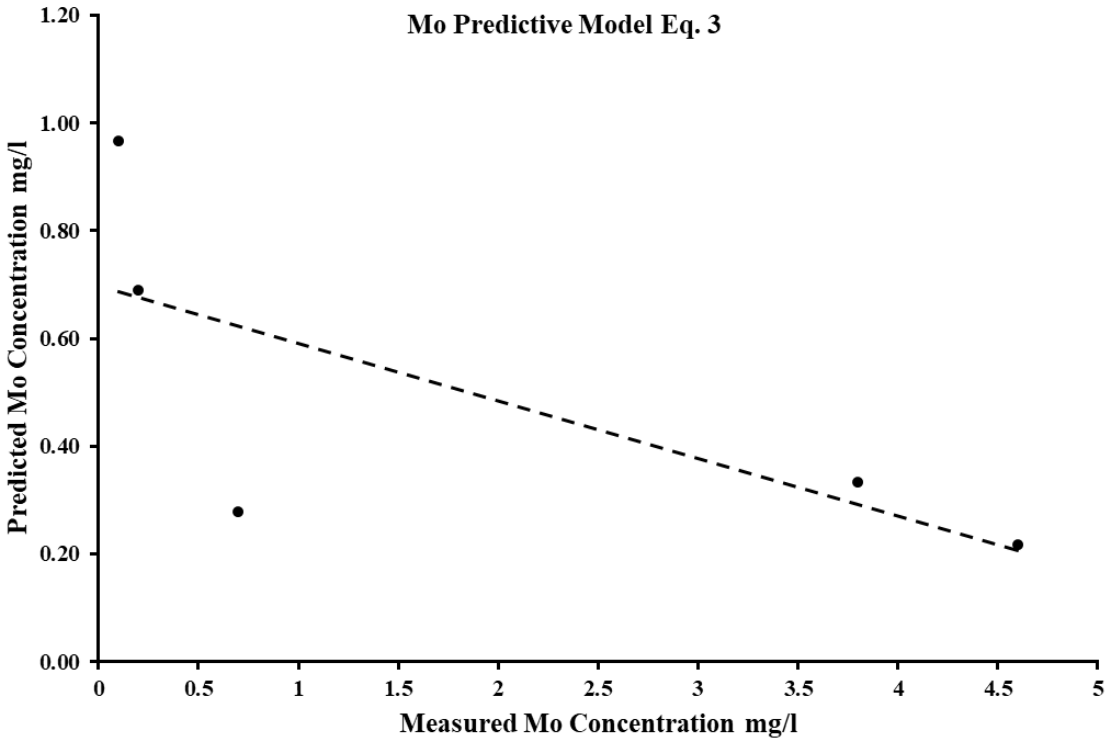

Figure 10 Accuracy assessment of the Mo predictive model for Eq. (3).

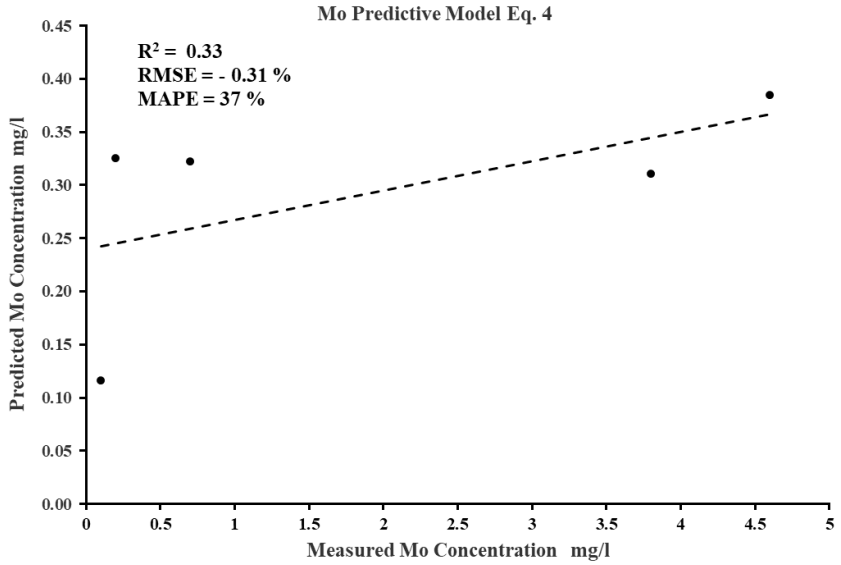

Figure 11 Accuracy assessment of the Mo predictive model for Eq. (4).

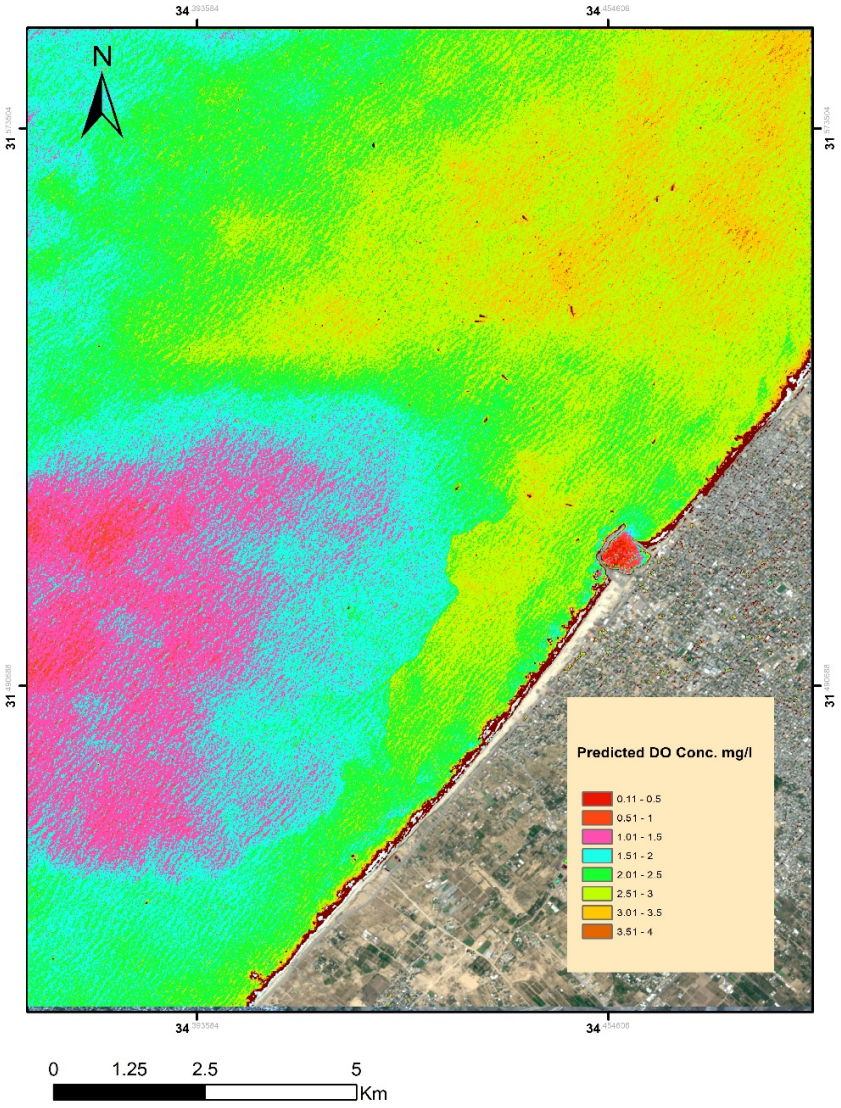

Figure 12 Distribution of DO concentration in the coastal zone of the Gaza Strip, using the developed predictive DO model based on Eq. (1). The predictive DO model was applied to Sentinel-2B Level 1C imagery, captured on December 31, 2020.

The DO map, **Figure 12**, highlights the severe impact of wastewater discharges on water quality, leading to hypoxic conditions in certain regions. It shows that the lowest oxygen concentrations are found in the fishing basin, a stagnant water area with limited water renewal. Additionally, the presence of petrochemicals and fuels in this area further reduces the water's suitability for marine life. The image also reveals varying patterns of DO distribution, with the movement of the current flowing from the west of the port to the north. This pattern supports the effectiveness of the prediction model in accurately estimating DO concentrations. Conversely, the Mo distribution map, **Figure 13**, points to localized contamination near coastal infrastructure, which is linked to erosion and degradation of construction materials and steel commonly used in coastal groins and coastal structures.

In contrast, the nearshore coastal water showed little to no presence of molybdenum. Despite the model's average performance in accuracy assessment tests, the Mo predictive model demonstrated a reasonable capability for predicting the dispersion of Mo in coastal waters. These findings highlight the potential of remote sensing as a tool for examining and assessing various non-optically active elements, suggesting that further evaluation and enhancement through future research would be beneficial.

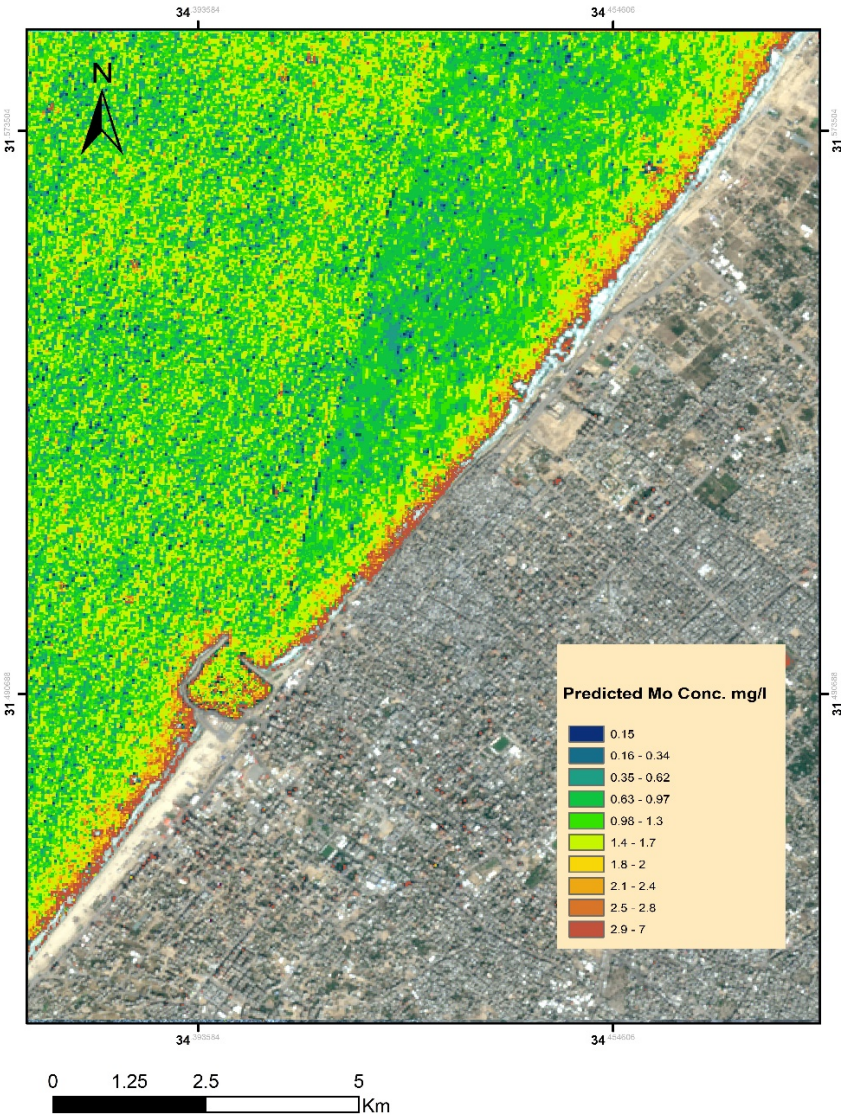

Figure 13 Distribution of Mo concentration in the coastal zone of the Gaza Strip, using the developed predictive Mo model based on Eq. (3). The predictive Mo model was applied to Sentinel-2B Level 1C imagery, captured on December 31, 2020.

4. Conclusions

This study demonstrated the potential of remote sensing for assessing coastal water quality by developing empirical predictive models for DO and Mo concentrations in the Gaza Strip. The models, built using Sentinel-2 multispectral reflectance data, successfully highlighted the spatial distribution of these non-optically active elements, offering valuable insights for environmental monitoring. However, the accuracy of the Mo model was lower due to the inherent challenges of modeling low-concentration elements.

The key findings of this study are:

4.1 DO model: The DO predictive model showed strong accuracy, with a high R^2 value and low error metrics (RMSE and MAPE), making it effective in identifying hypoxic areas in coastal waters, particularly near wastewater discharge zones. This demonstrates the model's ability to capture critical environmental stressors, such as pollution from untreated wastewater, which leads to low oxygen levels harmful to marine life.

4.2 Mo model: The Mo model, while informative, exhibited lower predictive accuracy. This was reflected in its lower R^2 values and higher error margins. This finding underscores the challenges of predicting non-optically active elements, particularly in areas with complex pollution sources and low-concentration elements like Mo.

Despite these challenges, the study successfully developed and applied empirical models that demonstrated the utility of remote sensing techniques for water quality monitoring. The prediction maps revealed distinct spatial patterns of contamination, particularly in areas surrounding the Gaza Fishing Port, Al-Shati Camp, and sewage outlets, highlighting the impact of human activity and coastal development on water quality.

The results of this study emphasize the importance of remote sensing as an efficient tool for large-scale, cost-effective environmental monitoring. By correlating satellite spectral reflectance with in-situ measurements, these predictive models provide a rapid method for assessing seawater quality, especially for non-optically active elements like DO and Mo. While Sentinel-2 data proved valuable for modeling DO with reasonable accuracy, the Mo model requires further refinement.

5. Challenges and future research

The study highlights the difficulties in predicting low-concentration, non-optically active elements using satellite data. For elements like Mo, which have weaker correlations with spectral reflectance, future research could explore several avenues to improve predictive accuracy. One of the possible strategies to improve non-optical active constituents monitoring is incorporating additional spectral bands from other satellite platforms and integrating environmental variables, such as temperature and salinity, to enhance model predictions. Additionally, expanding the spatial and temporal scope of in-situ data collection, especially in areas with varied pollution sources, could improve model reliability and generalizability.

Acknowledgment

The author would like to thank the Faculty of Applied Sciences and Technology, University Tun Hussein Onn Malaysia, Pagoh Campus, for providing facilities for this research. This study was supported by the Postgraduate Research Grant (GPPS) from the Universiti Tun Hussein Onn Malaysia (UTHM) (Code No. Q575). It is part of a thesis that will be submitted as partial fulfillment to meet the requirements for the Degree of Doctor of Philosophy at UTHM.

References

Abualhin, K., & Niemeyer, I. (2018). Deriving bathymetric maps of the shallow coastal water of the Gaza Strip Coastal Zone using passive remotely sensed imagery. *Journal of the Indian Society of Remote Sensing 46*(9), 1341-1351. https://doi.org/10.1007/s12524-018-0778-y

Abualtayef, M., Rabou, M. A., Afifi, S., Rabou, A. F. A., Seif, A. K., & Masria, A. (2021). Change

detection of Gaza Coastal Zone using GIS and remote sensing techniques. *Journal of Coastal Conservation, 25*(3), 36. https://doi.org/10.1007/s11852-021-00825-4

Brezonik, P. L., Olmanson, L. G., Finlay, J. C., & Bauer, M. E. (2015). Factors affecting the measurement of CDOM by remote sensing of optically complex inland waters. *Remote Sensing of Environment, 157*, 199-215. https://doi.org/10.1016/J.RSE.2014.04.033

Chapman, D. V., WHO, UNESCO, & UNEP. (1996). *Water quality assessments: A guide to use of biota, sediments and water in environmental monitoring.* In Chapman, D. V. (2nd eds.). Vol. 2. London: E & FN Spon.

Dierssen, H. M. (2010). Perspectives on empirical approaches for ocean color remote sensing of chlorophyll in a changing climate. *Proceedings of the National Academy of Sciences of the United States of America, 107*(40), 17073-17078. https://doi.org/10.1073/pnas.0913800107

Doxaran, D., Froidefond, J. M., & Castaing, P. (2002). A reflectance band ratio used to estimate suspended matter concentrations in sediment-dominated coastal waters. *International Journal of Remote Sensing, 23*(23), 5079-5085. https://doi.org/10.1080/0143116021000009912

Eaton, A. D., Clesceri, L. S., Greenberg, A. E., Franson, M. A. H., American Public Health Association, American Water Works Association, & Water Environment Federation. (2012). *Standard methods for the examination of water and wastewater*. American Public Health Association.

ESA. (2021). Level-1C product formatting - Sentinel-2 MSI technical guide - Sentinel online - Sentinel online. Retrieved from https://sentinels.copernicus.eu/web/sentinel/technical-guides/sentinel-2-msi/level-1c-processing

Ferdous, J., & Rahman, M. T. U. (2020). Developing an empirical model from landsat data series for monitoring water salinity in coastal Bangladesh. *Journal of Environmental Management,* 255(10), 109861. https://doi.org/10.1016/j.jenvman.2019.109861

Fu, B., Lao, Z., Liang, Y., Sun, J., He, X., Deng, T., He, W., Fan, D., Gao, E., & Hou, Q. (2022). Evaluating optically and non-optically active water quality and its response relationship to hydro-meteorology using multi-source data in Poyang Lake, China. *Ecological Indicators, 145*, 109675. https://doi.org/10.1016/j.ecolind.2022.109675

Gholizadeh, M. H., & Melesse, A. M. (2017). Study on spatiotemporal variability of water quality parameters in Florida Bay using remote sensing. *Journal of Remote Sensing & GIS,* 6(3), 1-11. https://doi.org/10.4172/2469-4134.1000207

Gons, H. J. (1999). Optical teledetection of chlorophyll a in Turbid Inland Waters. *Environmental Science and Technology, 33*(7), 1127-1132. https://doi.org/10.1021/es9809657

González-Márquez, L. C., Torres-Bejarano, F. M., Torregroza-Espinosa, A. C., Hansen-Rodríguez, I. R., & Rodríguez-Gallegos, H. B. (2018). Use of LANDSAT 8 images for depth and water quality assessment of El Guájaro Reservoir, Colombia. *Journal of South American Earth Sciences, 82*, 231-238. https://doi.org/10.1016/j.jsames.2018.01.004

Guo, H., Huang, J. J., Chen, B., Guo, X., & Singh, V. P. (2021). A machine learning-based strategy for estimating non-optically active water quality parameters using Sentinel-2 imagery. *International Journal of Remote Sensing, 42*(5), 1841-1866. https://doi.org/10.1080/01431161.2020.1846222

Gupta, R. P. (2017). *Remote sensing geology* (3rd eds.). Vol. 33. Springer Verlag. https://doi.org/10.1007/978-3-662-55876-8

Hassan, G., Goher, M. E., Shaheen, M. E., & Taie, S. A. (2021). Hybrid predictive model for water quality monitoring based on Sentinel-2A L1C data. *IEEE Access, 9*, 65730-65749. https://doi.org/10.1109/ACCESS.2021.3075849

Karaoui, I., Abdelghani, B., Arioua, A., Hssaisoune, M., Sabri, M., Ouhamchich, K. A., Elhamdouni, D., Idrissi, A. E. A., & Nouaim, W. (2019). Evaluating the potential of Sentinel-2 satellite images for water quality characterization of artificial reservoirs: The Bin

El ouidane reservoir case study (Morocco). *Meteorology Hydrology and Water Management, 7*(1), 31-39. https://doi.org/10.26491/mhwm/95087

Kim, C., Eom, J. B., Jung, S., & Ji, T. (2016). Detection of organic compounds in water by an optical absorbance method. *Sensors (Switzerland), 16*(1), 1-7. https://doi.org/10.3390/s16010061

Lubczonek, J., & Zaniewicz, G. (2023). Application of filtering techniques to smooth a surface of hybrid digital bathymetric model. *Remote Sensing, 15*(19), 4737. https://doi.org/10.3390/rs15194737

Mathew, M. M., Rao, N. S., & Mandla, V. R. (2017). Development of regression equation to study the total nitrogen, total phosphorus and suspended sediment using remote sensing data in Gujarat and Maharashtra Coast of India. *Journal of Coastal Conservation, 21*(6), 917-927. https://doi.org/10.1007/s11852-017-0561-1

Matthews, M. W. (2011). A current review of empirical procedures of remote sensing in Inland and Near-Coastal Transitional Waters. *International Journal of Remote Sensing, 32*(21), 6855-6899. https://doi.org/10.1080/01431161.2010.512947

McKee, D., Cunningham, A., & Dudek, A. (2007). Optical water type discrimination and tuning remote sensing band-ratio algorithms: Application to retrieval of chlorophyll and Kd(490) in the Irish and Celtic Seas. *Estuarine, Coastal and Shelf Science, 73*(3-4), 827-834. https://doi.org/10.1016/j.ecss.2007.03.028

Meer, F. D. V. D., Werff, H. M. A. V. D., & Ruitenbeek, F. J. A. V. (2014). Potential of ESA's Sentinel-2 for geological applications. *Remote Sensing of Environment, 148*, 124-133. https://doi.org/10.1016/j.rse.2014.03.022

Morel, A., & Gentili, B. (2009). Remote sensing of environment a simple band ratio technique to quantify the colored dissolved and detrital organic material from ocean color remotely sensed data. *Remote Sensing of Environment, 113*(5), 998-1011. https://doi.org/10.1016/j.rse.2009.01.008

Morrison, S. J., Mushovic, P. S., & Niesen, P. L. (2006). Early breakthrough of molybdenum and uranium in a permeable reactive barrier. *Environmental Science and Technology, 40*(6), 2018-2024. https://doi.org/10.1021/ES052128S

Mushtaq, F., & Lala, M. G. N. (2017). Remote estimation of water quality parameters of Himalayan Lake (Kashmir) using landsat 8 OLI imagery. *Geocarto International, 32*(3), 274-285. https://doi.org/10.1080/10106049.2016.1140818

Nahhal, D. E., El-Nahhal, I., Najar, H. A., Al-Agha, M., & El-Nahhal, Y. (2021). Acidity, electric conductivity, dissolved oxygen total dissolved solid and salinity profiles of marine water in Gaza: Influence of wastewater discharge. *American Journal of Analytical Chemistry, 12*(11), 408-428. https://doi.org/10.4236/ajac.2021.1211025

OCHA. (2018). Seawater pollution raises concerns of waterborne diseases and environmental hazards in the Gaza Strip: United Nations Office for the Coordination of Humanitarian Affairs - Occupied Palestinian Territory. *The United Nations Office for the Coordination of Humanitarian Affairs*. Retrieved from https://www.ochaopt.org/content/seawater-pollution-raises-concerns-waterborne-diseases-and-environmental-hazards-gaza-strip

Pizani, F. M. C., Maillard, P., Ferreira, A. F. F., & Amorim, C. C. D. (2020). Estimation of water quality in a reservoir from Sentinel-2 Msi and Landsat-8 Oli Sensors. *ISPRS Annals of the Photogrammetry, Remote Sensing and Spatial Information Sciences, 5*(3), 401-408. https://doi.org/10.5194/isprs-Annals-V-3-2020-401-2020

PWA. (2012). *Annual status report on water resources, water supply, and wastewater in the occupied State of Palestine 2011* (pp. 1-97). Palestinian Water Authority, State of Palestine.

Salomon, M., & Markus, T. (2018). *Handbook on marine environment protection*. In Salomon, M., & Markus, T. (Ed.). Springer International Publishing AG. https://doi.org/10.1007/978-3-319-60156-4

Segl, K., Guanter, L., Gascon, F., Kuester, T., Rogass, C., & Mielke, C. (2015). S2eteS: An end-to-end modeling tool for the simulation of Sentinel-2 image products. *IEEE Transactions on Geoscience and Remote Sensing, 53*(10), 55608-5571. https://doi.org/10.1109/TGRS.2015.2424992

Shomar, B. H., Müller, G., & Yahya, A. (2005). Seasonal variations of chemical composition of water and bottom sediments in the Wetland of Wadi Gaza , Gaza Strip. *Wetlands Ecology and Management, 13*(4), 419-431. https://doi.org/10.1007/s11273-004-0412-3

Smedley, P. L., & Kinniburgh, D. G. (2017). Molybdenum in natural waters: A review of occurrence, distributions and controls. *Applied Geochemistry, 84*, 387-432. https://doi.org/10.1016/j.apgeochem.2017.05.008

Sun, D., Qiu, Z., Li, Y., Shi, K., & Gong, S. (2014). Detection of total phosphorus concentrations of Turbid Inland Waters using a remote sensing method. *Water, Air, and Soil Pollution, 225*(5), 1-17. https://doi.org/10.1007/S11270-014-1953-6/METRICS

USEPA. (2012). *Recreational water quality criteria*. Washington, D.C.

Vestner, R. J., Brooke, K., & Nicolet-Misslbeck, L. (2013). Water reuse in the Gaza Strip, Palestine. *Water Science and Technology, 67*(4), 729-736. https://doi.org/10.2166/WST.2012.604

Wilcox, R. R. (2010). *Fundamentals of modern statistical methods: Substantially improving power and accuracy*. Vol. 249. New York: Springer.

Yu, X., Lee, Z., Shen, F., Wang, M., Wei, J., Jiang, L., & Shang, Z. (2019). An empirical algorithm to seamlessly retrieve the concentration of suspended particulate matter from water color across ocean to Turbid River Mouths. *Remote Sensing of Environment, 235*, 1-38. https://doi.org/10.1016/j.rse.2019.111491

Zeng, S., Li, Y., Lyu, H., Xu, J., Dong, X., Wang, R., Yang, Z., & Li, J. (2020). Mapping spatio-temporal dynamics of main water parameters and understanding their relationships with driving factors using GF-1 Images in a clear reservoir. *Environmental Science and Pollution Research, 27*(27), 33929-33950. https://doi.org/10.1007/s11356-020-09687-z